RSC Advances

PAPER

View Article Online
View Journal | View Issue

Cite this: *RSC Adv.*, 2015, **5**, 39416

Mechanical properties and variation in SOC going from La to Nd in intermetallic RIn_3 and RSn_3 (R = La, Ce, Pr, Nd)

M. Shafiq,[ab] Iftikhar Ahmad*[ab] and S. Jalali-Asadabadi*[c]

Received 28th February 2015
Accepted 8th April 2015

DOI: 10.1039/c5ra03597j

www.rsc.org/advances

First principle studies of the cubic rare-earth intermetallics RIn_3 and RSn_3 (R = La, Ce, Pr, Nd) have been carried out within the framework of density functional theory using the full potential linearized augmented plane waves plus local orbital method (FP-LAPW + lo). The calculated structural parameters with different functionals are found to be consistent with the experimental results. The effect of the Hubbard potential on the density of states is discussed in detail. It is observed that the inclusion of spin–orbit coupling (SOC) causes degeneracies of the electronic band structures in the vicinity of the Fermi level of these compounds. Furthermore, the SOC effect enhances as one goes from La to Nd in a compound, which demonstrates the interesting nature of this effect in the periodic table. The elastic constants, bulk moduli, shear moduli, Young's moduli, anisotropy, Kleinman parameters, Poisson's ratios, sound velocities for shear and longitudinal waves, and Debye temperatures are calculated and discussed, which reveal that these compounds are ductile in nature.

I. Introduction

Rare-earth (RE) intermetallic compounds are strongly correlated electron systems, and in this family of compounds RX_3 (R = rare-earth and X = In, Sn) are most exciting due to their interesting physics. The RX_3 compounds have attracted both experimental and theoretical attention because of their diverse bulk properties, such as low superconducting transition temperature, magnetic susceptibility and thermoelectric power as a function of their electron concentration.[1,2] These compounds offer many possibilities by replacing the X atom (X = In, Sn, Tl, Pb, *etc.*), and their single crystals can be easily grown due to their congruent melting.[3] Many of the RX_3 compounds crystallize in a cubic symmetry which is a more favorable structure for superconductivity than a lower symmetry.[4] Furthermore, these compounds are stable in the cubic structure at standard temperature and pressure (STP) and remain stable over a wide range of pressures.[5] In RSn_3 solders (Sn-solder) the rare-earth elements La, Ce, Er and Eu are used which are suitable replacements for Pb–Sn solder.[6] The amount of the RE element in Sn-solder improves both the physical and mechanical properties and in particular, enhances the ductility of the solder.[7]

Due to unfilled 4f orbitals and spin–orbit interactions, the adjacent electronic states strongly interact with each other, therefore the characterization of accurate physical properties and the development of analytical and computational tools for lanthanide-based compounds is a challenging problem for both experimental and theoretical researchers.[8] RX_3 (R = La, Ce, Pr and Nd, X = In and Sn) intermetallic compounds crystallize in the cubic $AuCu_3$-type crystal structure with space group $Pm\bar{3}m$ (no. 221). The point groups of the R and X atoms are cubic $m\bar{3}m$ and non-cubic $4/mmm$, respectively.[9] In the RX_3 compounds, the valency of the lanthanide can be inferred from lattice constant measurement techniques. The lattice constant of R^{2+} is larger than R^{3+} by almost 10% for pure lanthanides.[10] For diluted lanthanides RX_3 (R = Eu, Yb) (addition of other elements with the lanthanides), the lattice constant increases by less than 2% when compared to other RX_3 compounds. This shows the unusual nature of Eu and Yb, which display divalency in this 4f series of compounds.[9,11] Most of the RIn_3 and RSn_3 compounds are antiferromagnetic (AFM)[12,13] except Pauli paramagnetic $LaIn_3$, and paramagnetic $LaSn_3$, $CeSn_3$ and $PrIn_3$.[14–16] The AFM transition Néel temperatures (T_N) for $CeIn_3$, $NdIn_3$, $PrSn_3$ and $NdSn_3$ are 10 K, 5.9 K, 8.6 K, and 4.7 K, respectively.[17–19] Some RIn_3 and RSn_3 compounds exhibit superconductivity. The superconducting transition temperatures (T_C) for $LaIn_3$, $LaSn_3$ and $CeIn_3$ are 0.71 K, 6.5 K, and 0.2 K, respectively.[20,21] Moreover, $CeIn_3$ and $PrSn_3$ are heavy fermion compounds.[22,23] Due to both the localized and itinerant character of the f electrons, $CeIn_3$ is also described as mixed valence or intermediate valence[24] and $CeSn_3$ is categorized as a Kondo compound with valence fluctuation.[25] The Fermi surface properties and the de

[a]*Center for Computational Materials Science, University of Malakand, Pakistan. E-mail: ahma5532@gmail.com; Tel: +92-332-906-7866*

[b]*Department of Physics, University of Malakand, Chakdara, Pakistan*

[c]*Department of Physics, Faculty of Science, University of Isfahan, Hezar Gerib Avenue, Isfahan 81746-73441, Iran. E-mail: saeid.jalali.asadabadi@gmail.com; sjalali@sci.ui.ac.ir; Tel: +98 9133287908*

Haas–van Alphen (dHvA) effect in RX_3 compounds were reported by Ōnuki and Settai,[26] whereas the pressure dependent electronic structure and optical conductivity of the $CeIn_3$ compound in the AFM phase were experimentally investigated by Iizuka *et al.*[27]

Some theoretical studies on the pressure dependent structural, electronic and elastic properties of the intermetallic compounds $LaIn_3$, $LaSn_3$, $CeIn_3$ and $CeSn_3$ are available[1,2,28,29] in the literature but their theoretical results are not consistent with the experiments because of the improper treatment of the exchange-correlation potential in those calculations. In these studies, they have used local density approximation (LDA) and generalized gradient approximation (GGA) where it is evident that RIn_3 and RSn_3 compounds are strongly correlated electron systems with 4f electrons. Therefore, to obtain the rational and logical electronic structures and other physical properties of these compounds, it is necessary to treat the strong correlation effects by an additional local Hubbard repulsion of magnitude U, *i.e.*, DFT + U techniques as well as spin–orbit coupling (SOC) effects to increase the accuracy of the calculated results. These deliberations have been considered in carrying out the calculations of the structural, electronic, elastic and mechanical properties of the intermetallic compounds, RX_3 (R = La, Ce, Pr and Nd, X = In and Sn). The calculations are carried out using the full potential linearized augmented plane waves plus local orbitals (FP-LAPW + lo) method under the framework of DFT. We have carried out these studies with the motivation that the elastic and mechanical properties of $CeIn_3$, $CeSn_3$, $PrIn_3$, $PrSn_3$, $NdIn_3$ and $NdSn_3$ have never been explored, neither theoretically nor experimentally, which may be promising materials with improved mechanical properties for practical applications. This study will cover the missing information in the literature about these materials and will also provide the basis for future experiments.

II. Method of calculations

The calculations have been performed by using density functional theory (DFT) implemented in the WIEN2k code[30] and employing the full potential linearized augmented plane waves plus local orbitals (FP-LAPW + lo) method.[31] The exchange-correlation effects are calculated within the local density approximation (LDA),[32] generalized gradient approximation (GGA),[33] GGAsol,[34] Wu–Cohen GGA (WC-GGA),[35] meta GGA (m-GGA)[36] and hybrid functional B3PW91 [37,38] with spin polarization. As lanthanides are strongly correlated systems with localized 4f electrons,[39,40] to obtain the exact nature of the electronic structure of the compounds under consideration, we used LDA + U and GGA + U methods. The DFT + U method is based on the Hubbard model, which treats the strongly correlated electron systems with an orbital dependent potential of Coulomb and exchange interactions.[41] The optimized values of the U parameter are obtained by varying U, step by step. After examining several values for the U parameter, values were selected which gave better results for the magnetic moment in comparison with the experimental values for the corresponding compounds. The values of U used within the calculations are given in Table 1. One can clearly see a trend of increasing U with increasing atomic number. This is because with increasing atomic number, the f state becomes deeper and the orbitals become more localized, thus leading to an increased Coulomb interaction. Furthermore, spin–orbit coupling (SOC) is included to treat the relativistic effects. The SOC values are included using a second variational method.[42] The second variational method, which makes use of the scalar-relativistic basis, is based on the reduction of the original basis. In the first step of this approach, the scalar-relativistic part of the Hamiltonian is diagonalized in the scalar-relativistic basis. In the second step, the full Hamiltonian matrix including SOC is constructed using the eigenfunctions of the first step Hamiltonian. Once the effects of the spin–orbit coupling are included, then the full Hamiltonian can be written as:

$$H\tilde{\psi} = \varepsilon\tilde{\psi} + H_{so}\tilde{\psi} \quad (1)$$

where, H_{so} is the spin–orbit Hamiltonian and is given by:[43]

$$H_{so} = \frac{\hbar}{2Mc^2}\frac{1}{r}\frac{dV}{dr}\begin{pmatrix} \vec{\sigma}\cdot\vec{l} & 0 \\ 0 & 0 \end{pmatrix} \quad (2)$$

where $\vec{\sigma}$ represents the Pauli spin matrices.

The radii of the muffin-tin spheres have been chosen as 2.50 au. for the rare-earth elements as well as for Sn and In. To achieve convergence, the basis set is expanded in terms of plane waves up to $R_{MT}K_{max} = 7$ where R_{MT} is the smallest atomic radius in a unit cell and K_{max} is the magnitude of the maximum value of the k-vector in the plane waves expansion. For the valence wave function inside muffin-tin spheres, the maximum value of the angular momentum $l_{max} = 10$ is considered. In the interstitial region, the charge density is Fourier expanded up to $G_{max} = 12$. High accuracy is required to calculate elastic properties, therefore by increasing the number of k-points, we tested the convergence of the total energy and hence the total energy is converged for 6000 k-points with a dense k mesh of 165 k-points in the irreducible wedge of the Brillouin zone with a grid size of $18 \times 18 \times 18$ using the Monkhorst and Pack mesh.[44]

The elastic constants of RX_3 are calculated with Cubic-elastic software,[45] using the energy approach[46] implemented in the WIEN2k code. In this work Voigt notations are replaced, which the number of elastic constants and hence for a cubic lattice only three independent elastic constants C_{11}, C_{12} and C_{44} are left, which can be determined by introducing orthorhombic, cubic and monoclinic lattice distortions.[47] These constants are calculated, and are further used to evaluate the mechanical properties of RX_3 such as the shear modulus (G), Young's modulus (Y), Cauchy pressure (C''), Poisson's ratio (ν), Kleinman parameter (ξ), and anisotropy constant (A) using standard relations.[47,48]

Table 1 Values of U used for RIn_3 and RSn_3

Comp.	$LaIn_3$	$CeIn_3$	$PrIn_3$	$NdIn_3$	$LaSn_3$	$CeSn_3$	$PrSn_3$	$NdSn_3$
U (eV)	5.0	5.5	5.8	6.2	5.0	5.5	5.8	6.2

III. Results and discussion

A. Ground state structural properties

The ground state structural properties of RX_3 (R = La, Ce, Pr and Nd, X = In and Sn) are calculated by finding the total energy of the unit cell for each compound with respect to volume using the Birch–Murnaghan equation of state.[49] The lattice constant (a) and zero pressure bulk moduli (B_0) are determined using a variety of schemes including LDA, GGA, GGAsol, WC-GGA, LDA + U, GGA + U, and meta-GGA (m-GGA), as well as B3PW91 hybrid functionals.

The theoretically calculated results of the lattice constants and bulk moduli along with the available experimental data are listed in Tables 2 and 3, respectively.

The calculated GGA, GGA + U and m-GGA lattice constants are slightly larger than those of GGAsol, WC-GGA, LDA + U and B3PW91, while the calculated values for the bulk moduli by GGA, GGA + U and m-GGA for these compounds are smaller than those of the GGAsol and WC-GGA and B3PW91. This confirms the general trend of these approximations, that GGA overestimates and LDA underestimates lattice constants.[34] Table 2 indicates that the computed lattice constants using the B3PW91 hybrid functional are in better agreement with the experimental values than the other theoretical approaches. It is also clear from the table that B3PW91 is the best performing functional for strongly correlated systems as compared to the other schemes. Table 2 also shows that as we move from La to Nd, the lattice constants are contracted, which can be attributed to the lanthanide contraction, *i.e.*, the decrease in the atomic radius along the lanthanide series from left to right due to the poor shielding effect of the 4f electrons. Table 3 shows that the calculated bulk moduli using B3PW91 for all of the compounds are very close to each other and lie in the range of 52.950 and 70.686 GPa. This trend of the bulk moduli is also evident from the calculated results using GGAsol, GGA, m-GGA WC-GGA and LDA + U. No experimental data to the best of our knowledge is available for the bulk moduli, so our results are considered as a prediction for these properties of RIn_3 and RSn_3 (R = La, Ce, Pr and Nd) compounds.

B. Electronic structure and density of states

In order to reveal the electronic band structure, the spin polarized total density of states (TDOS) and 4f density of states are calculated by employing GGA and LDA for the exchange and correlation functional. The DOSs calculated by GGA and LDA approximations are quite similar and only the GGA density of states and 4f-DOSs for RIn_3 and RSn_3 (R = La, Ce, Pr and Nd, X = In and Sn) are presented in Fig. 1, where the Fermi level is set at 0 eV. It is clear from the figure that no band gap is available at the Fermi level for any of the intermetallic compounds under consideration; hence all of these compounds are metallic in nature. The figure also reveals the dominating character of the f state in all of these compounds. It is also evident from the figure that no prominent peak occurs at the Fermi level for any of these compounds under study; therefore all of these compounds are ductile in nature. The maximum peaks of $LaIn_3$ and $LaSn_3$ are above the Fermi level in the unoccupied states around 2.74 eV and 2.95 eV, respectively. Therefore, the $LaIn_3$ and $LaSn_3$ compounds show more ductility than the remaining RIn_3 and RSn_3 compounds, which is due to the large separation between the Fermi level and the f states according to a previous study.[50]

Strongly correlated systems such as lanthanides (and actinides)[39,51] which involve 4f (or 5f) orbitals have interesting physical and chemical properties, because these electrons can be localized or itinerant depending on the crystalline environment. Therefore, to understand the effects of the 4f orbitals in these compounds, the calculations are also carried out with the Hubbard potential U (GGA + U and LDA + U). The total density of states (TDOSs) with GGA + U and partial density of states (DOSs) of the f states, as well as the TDOS with GGA, are plotted in Fig. 2. It is clear from the figure that both GGA and GGA + U provide different DOSs. The differences in the DOSs for all of the compounds can be clearly seen from the figure. The figure clearly indicates that the strong peaks which are due to the 4f states are significantly shifted up and down by the application of the Hubbard potential (U) as compared to the GGA scheme. This is in agreement with previous DFT calculations which show the Hubbard potential opens the gap between the occupied and unoccupied states.[52]

Spin–orbit coupling (SOC), which was apparently a weak relativistic correction to the Schrödinger equation in condensed matter physics, has recently attracted enormous attention in modern condensed-matter physics because of its key role in 5d, 4f and 5f electronic states. The spin and orbital degrees of freedom are entangled at a local level by the SOC, where the

Table 2 The calculated values of the lattice parameters (a in Å) of RIn_3 and RSn_3 (R = La, Ce, Pr and Nd) compounds

Comp.	LDA	GGAsol	GGA	WC	LDA + U	GGA + U	B3PW91	m-GGA	Exp.
$LaIn_3$	4.645	4.697	4.787	4.704	4.698	4.835	4.738	4.789	4.732[a]
$CeIn_3$	4.554	4.601	4.718	4.609	4.612	4.761	4.676	4.708	4.687[a]
$PrIn_3$	4.546	4.605	4.705	4.617	4.647	4.795	4.669	4.701	4.670[a]
$NdIn_3$	4.540	4.603	4.689	4.609	4.626	4.765	4.647	4.696	4.653[a]
$LaSn_3$	4.686	4.728	4.816	4.736	4.738	4.864	4.773	4.815	4.769[b]
$CeSn_3$	4.589	4.626	4.755	4.637	4.636	4.785	4.710	4.749	4.721[b]
$PrSn_3$	4.582	4.632	4.729	4.647	4.661	4.839	4.709	4.734	4.716[b]
$NdSn_3$	4.581	4.624	4.713	4.637	4.644	4.776	4.701	4.713	4.705[b]

[a] Ref. 13. [b] Ref. 66.

Table 3 The calculated value of the bulk moduli (B_0 in GPa) of RIn_3 and RSn_3 (R = La, Ce, Pr and Nd) compounds

Comp.	LDA	GGAsol	GGA	WC	LDA + U	GGA + U	B3PW91	m-GGA
$LaIn_3$	60.816	58.184	52.293	58.653	60.188	53.720	56.213	52.157
$CeIn_3$	74.382	63.580	52.703	63.166	61.029	51.628	61.100	50.536
$PrIn_3$	63.110	61.015	53.319	61.106	54.015	59.587	53.044	54.791
$NdIn_3$	63.493	61.943	52.527	59.278	69.926	49.240	64.591	49.120
$LaSn_3$	65.837	60.339	53.861	59.064	61.507	56.910	55.646	50.004
$CeSn_3$	79.210	71.621	67.212	71.920	71.445	55.026	70.686	60.948
$PrSn_3$	70.565	66.817	52.580	64.541	67.438	52.322	55.720	49.704
$NdSn_3$	72.514	62.381	56.295	66.712	69.969	51.222	52.950	51.046

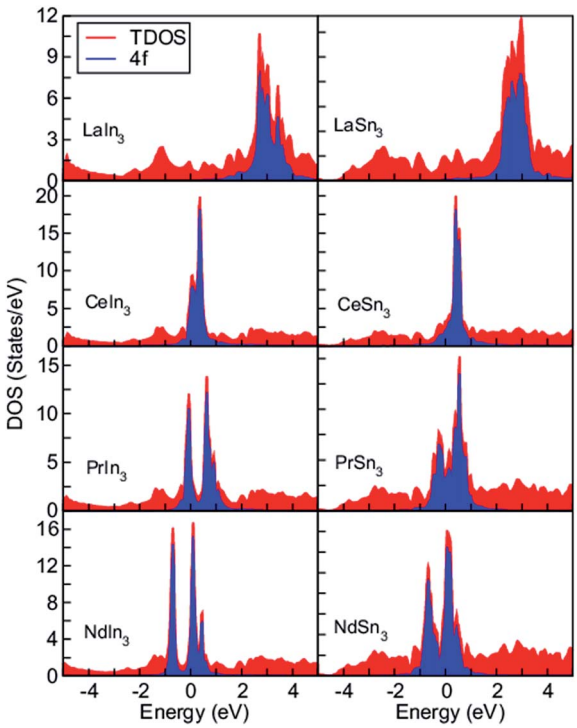

Fig. 1 Total density of states TDOSs (red shading) and partial 4f-DOSs (blue shading) of RIn_3 and RSn_3 for R = La, Ce, Pr and Nd calculated with GGA.

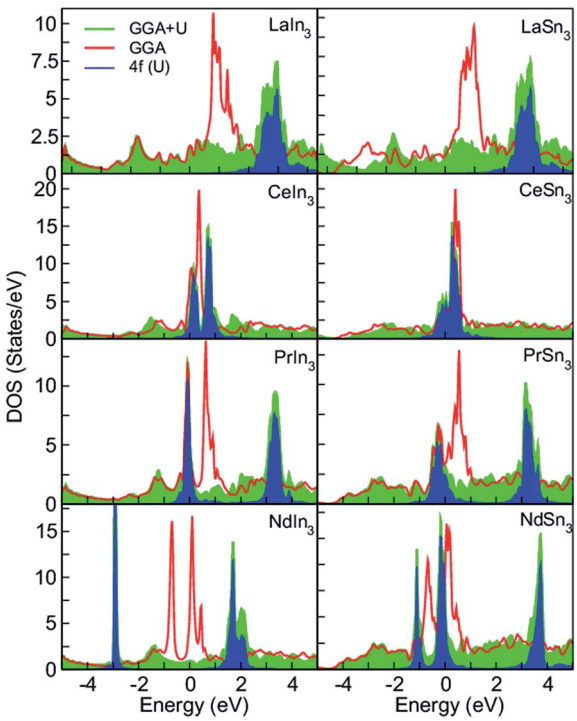

Fig. 2 Total density of states (TDOSs) with GGA (red lines), GGA + U (green shading) and PDOSs GGA + U-4f of RIn_3 and RSn_3 for R = La, Ce, Pr and Nd.

total angular momentum provides a good description of the ordered phases and fluctuation properties of a material and can also describe the possible uses of a material in various devices with prominent functionalities.[53] To see the effect of the spin–orbit coupling (SOC) in the compounds under study their band structures along high symmetry directions with GGA and GGA + SOC are presented in Fig. 3. It is clear from the figure that the effect on the band structures of $LaIn_3$ and $LaSn_3$ is very small, which is in agreement with earlier work.[1,54] The comparison of the band structures of these compounds reveals that, as one moves from La to Nd, the effect of SOC increases. This might be due to the fact that as the Coulomb attraction on an electron in a particular orbit increases, from La to Nd in the periodic table, the orbit shrinks and hence the electron speeds up to conserve the momentum of the system, where with this increase in the speed the relativistic effects of SOC increase. The differences between the GGA and GGA + SOC band structures in the vicinity of the Fermi level are shown in the insets of each compound in Fig. 3 lifting some degeneracies in the band structures. The figure also shows that the band along the symmetry line between X and M in the $CeIn_3$ compound, dips below the Fermi level in the GGA scheme but stays above the Fermi level when SOC is introduced. The degeneracy in $PrIn_3$ is observed at the R symmetry line, whereas in $CeSn_3$ and $PrSn_3$, the degeneracies occur at the M symmetry line. The SOC effects can be clearly seen for different symmetry lines in $NdIn_3$ and $NdSn_3$.

C. Elastic and mechanical properties

The elastic constants of solids provide significant information about the nature of the forces operating in solids. Elastic constants are very important for understanding the relationship between the crystal structure and bonding nature. These

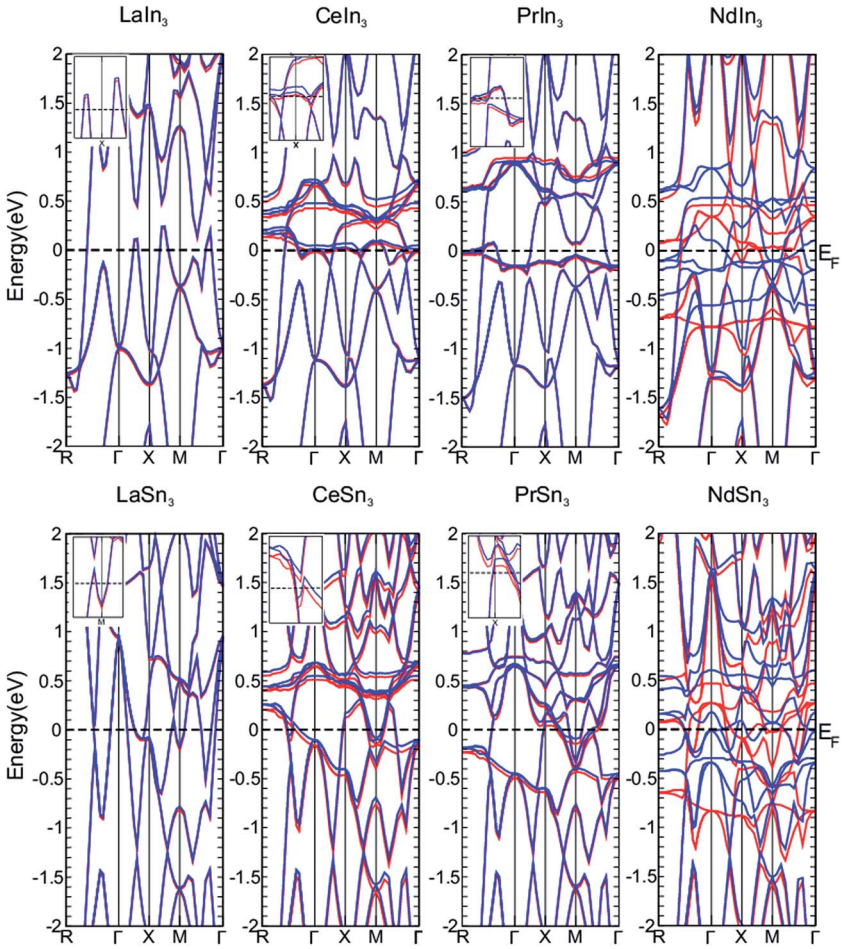

Fig. 3 Comparison of the electronic band structures calculated with GGA and GGA + SOC for RIn_3 and RSn_3. The red lines show band structures with GGA without SOC, while the blue lines show the band structures with SOC.

constants also reveal the structural stability and various other important physical properties of materials. The elastic constants C_{11}, C_{12}, and C_{44} for RIn_3 and RSn_3 (R = La, Ce, Pr and Nd) are calculated within GGA and GGAsol with spin polarization and are given in Table 4. The available experimental elastic constants (for $LaSn_3$) along with other theoretical results are also listed in the table. No experimental data is available for these compounds except $LaSn_3$. It is clear from the table that our calculated values for the elastic constants of the $LaSn_3$ compound with GGAsol are in excellent agreement with the

Table 4 The calculated values of elastic constants C_{11}, C_{12}, C_{44} (GPa) with GGAsol and (GGA)

Comp.	E_{XC}	$LaIn_3$	$CeIn_3$	$PrIn_3$	$NdIn_3$	$LaSn_3$	$CeSn_3$	$PrSn_3$	$NdSn_3$
C_{11}	GGAsol	89.265	95.500	83.878	82.569	69.273	99.084	80.343	87.167
	GGA	97.525	100.909	80.152	85.405	86.732	85.005	80.247	96.191
	Exp.					70.50[a]			
	Other					97.30[b], 83.17[c]			
C_{12}	GGAsol	42.555	45.609	37.137	41.498	42.328	53.678	38.842	34.211
	GGA	50.885	49.383	29.183	60.287	43.855	57.967	44.094	25.357
	Exp.					42.00[a]			
	Other					53.6[b], 45.51[c]			
C_{44}	GGAsol	27.280	29.879	32.365	35.340	27.584	48.904	28.575	30.375
	GGA	28.125	37.543	34.767	33.997	35.463	45.431	28.370	27.367
	Exp.					33.50[a]			
	Other					44.20[b], 31.22[c]			

[a] Ref. 55. [b] Ref. 1. [c] Ref. 28.

experimental results of Stassis *et al.*,[55] extracted from the phonon dispersion curves, as compared to other theoretical results reported in ref. 1 and 28. Hence, from the consistency of our calculated values with the experimental results for this compound, we infer that our calculated values for the remaining compounds under investigation will also be consistent with the corresponding experimental values. Moreover, the stability criteria initiated by Born[56] for cubic systems in terms of elastic constants, *i.e.*, $C_{11} - C_{12} > 0$, $C_{44} >$ and $C_{11} + 2C_{12} > 0$ are well satisfied by these compounds. The fulfillment of these criteria justifies that these intermetallic compounds are elastically stable.

The trend of the mechanical properties of a material could be estimated from its elastic constants. As the elastic constants C_{11}, C_{12}, and C_{44}, calculated by both GGA and GGAsol, exchange and correlation effects are very close to each other, therefore in this article the mechanical properties of the compounds are evaluated using the GGAsol results. The main mechanical parameters, *i.e.* shear modulus (G), Young's modulus (Y), Pugh's ratio (B/G), Cauchy's pressure (C''), Poisson's ratio (ν) and anisotropic ratio (A), which are important for industrial applications are calculated and presented in Table 5. These important parameters are used to characterize the mechanical behavior of a material.

The average Hill's[57] shear modulus, $G_H = G$, as a measure of resistance to plastic deformation upon shear stress is the arithmetic mean of the Reuss and Voigt shear moduli.[58,59] The values of G_H given in Table 5 indicate that $CeSn_3$ offers more resistance to plastic deformation than the remaining compounds. The Young's modulus (Y) defines the ratio between the linear stress and strain. The larger the value of Y, the stiffer the material will be. From Table 5 one can see that $CeSn_3$ has the largest Young's modulus value (stiffer). The higher values for the Young's moduli as compared to their bulk moduli confirm the stiffness of these compounds. The Hill's and shear moduli are further used to explain the ductile and brittle nature of a compound.

Pugh[60] suggested an index for the ductility and brittleness of a material. The Pugh's ratio (B/G) reflects the competition between the shear and cohesive strength of a material and describes its ductile/brittle character. If B/G is greater than the critical value 1.75, the material behaves in a ductile manner; otherwise the material will be brittle in nature. It is evident from Table 5, that the B/G ratio for all of the RIn_3 and RSn_3 compounds show a ductile behavior ($B/G > 1.75$). The larger values of B/G for $LaSn_3$ (2.412) and for $LaIn_3$ (2.267) reveal a higher degree of ductility. The same nature has also been observed in the DOSs plot (Fig. 1) for $LaSn_3$ and $LaIn_3$, showing that they have a more ductile nature than the other compounds. The ductile and brittle behavior of a compound can be also discussed in terms of the elastic constants C_{12} and C_{44}. The Cauchy's pressure ($C'' = C_{12} - C_{44}$) is used for this purpose and its positive/negative value shows the ductile/brittle behavior of a compound. The positive value of Cauchy's pressure (from Table 5) indicates that all of the compounds under investigation are ductile in nature, which confirms the results of the Pugh's B/G ratio. Cauchy's pressure is also used to indicate the bonding character of the compounds. The positive value of Cauchy's pressure is responsible for ionic bonding, while a material with negative Cauchy's pressure requires angular or directional character in bonding (covalent bonding). It is clear from Table 5 that all of the compounds possess positive Cauchy's pressure values, have metallic bonds and hence high mobility characteristics.

The Poisson's ratio ν usually quantifies the stability of a crystal against shear (compressibility). Its typical lower and upper bound limits are -1 and 0.5 respectively. The lower limit bound is where the material does not change its shape and the upper limit bound is where the volume remains unchanged.[61] Our calculated values for the Poisson's ratio lie between 0.313 and 0.265, which show that these materials are less compressible and stable against external deformation. The Poisson's ratio also demonstrates the ductile/brittle nature of a material. For ductile compounds $\nu \approx 0.3$ and for brittle $\nu > 0.35$. The Poisson's ratio for all of these compounds is less than 0.35, which further confirms the ductile nature of these compounds. Furthermore, the Poisson's ratio also gives information about bonding forces. For central forces in solids, the lower limit of ν is 0.25 and the upper limit of ν is 0.5.[62] The table shows that the calculated values of the Poisson's ratio fall within this limit and that the dominant interatomic forces are central forces.

The Kleinman internal strain parameter (ζ) describes the relative tendency of bond bending *versus* bond stretching.[63] Minimizing bond bending leads to $\zeta = 0$, while minimizing

Table 5 The calculated values of Voigt's shear modulus G_V, Reuss's shear modulus G_R, Hill's shear modulus G_H, Young's modulus Y, B/G ratio, Cauchy pressure (C''), Poisson's ratio (ν), Kleinman parameter (ζ), anisotropy constant (A), and shear constant (C')

Comp.	$LaIn_3$	$CeIn_3$	$PrIn_3$	$NdIn_3$	$LaSn_3$	$CeSn_3$	$PrSn_3$	$NdSn_3$
G_V	25.710	27.906	28.767	29.418	22.139	38.424	25.445	28.816
G_R	25.562	27.689	28.047	27.430	19.849	33.459	24.830	28.686
G_H	25.636	27.797	28.407	28.424	20.994	35.941	25.138	28.916
Y	67.219	72.832	73.020	74.939	57.971	97.183	65.749	72.940
B/G	2.267	2.239	1.856	1.942	2.412	1.915	2.095	1.794
C''	15.275	15.730	4.772	6.158	13.744	4.774	10.267	3.836
ν	0.307	0.305	0.269	0.274	0.309	0.265	0.292	0.266
ζ	0.796	0.797	0.743	0.838	0.994	0.902	0.807	0.666
A	1.168	1.198	1.385	1.721	1.974	2.154	1.377	1.147
C'	23.355	24.946	23.371	20.536	13.973	22.703	20.751	26.478

bond stretching leads to $\zeta = 1$. The calculated Kleinman parameters in Table 5 predict that in RIn_3 and RSn_3 compounds bond stretching is dominant (upper limit of ζ).

The anisotropic ratio (A) which measures the elastic anisotropy of a material is a very important property and is closely related to the induced microcracks in a material.[64] For an ideal isotropic material, the anisotropic ratio is unity and deviation from unity measures the amount of anisotropy. From Table 5 one can see that the value of the anisotropic ratio is found to be much greater than 1. The deviations from unity specify that these compounds are not elastically isotropic and their properties vary strongly in different directions.

The important parameter, which defines the dynamical stability of a material, is the shear constant C'. It is also one of the criterions of mechanical stability and shows the stability of the tetragonal distortion. Its values for the compounds under consideration are given in Table 5. The positive values of the shear constant ($C' > 0$) fulfill the required criteria for dynamical stability. From the calculated value of C' it is predicted that these compounds are dynamically stable materials.

D. Sound velocities and Debye temperatures

The thermo-physical properties like longitudinal v_l, transverse v_s, average sound velocities v_m, and Debye temperatures $\theta(D)$ of the compounds under study are also investigated. The Debye temperature $\theta(D)$ of a compound can be calculated using the following relationship:[65]

$$\theta(D) = \frac{h}{K_B}\left[\frac{3n}{4\pi}\left(\frac{N_A\rho}{M}\right)\right]^{1/3} v_m, \quad (3)$$

where h is the Plank's constant, K_B is the Boltzmann's constant, N_A is Avogadro's number, ρ is the density, M is the molecular weight, v_m is the average sound velocity and n is the number of atoms per formula unit. Similarly, the average sound velocity for any compound can be calculated using the following equation:

$$v_m = \left[\frac{1}{3}\left(\frac{2}{v_s^3} + \frac{1}{v_l^3}\right)\right]^{-1/3}, \quad (4)$$

where v_l and v_s are the longitudinal and transverse sound velocities which can be obtained in terms of the shear modulus G and the bulk modulus B_0 as:

$$v_l = \left[\frac{B + \frac{4G}{3}}{\rho}\right]^{1/2}, \text{ and } v_s = \left[\frac{G}{\rho}\right]^{1/2}. \quad (5)$$

The calculated theoretical densities, sound velocities and Debye temperatures are reported in Table 6. The calculated densities are in excellent agreement with the available experimental values in parentheses. A material with a greater Debye temperature will be stiffer and exhibit high thermal conductivity. Table 6 shows that $CeSn_3$ is stiffer than the other compounds ($\theta(D) = 151.05$), which confirms the result of the Young's modulus for $CeSn_3$ ($Y = 97.183$). The lower Debye temperature of $LaSn_3$ is a consequence of the lower elastic constant compared to the values of the rest of the compounds.

Table 6 The calculated values of densities ρ (g cm^{-3}), sound velocities of transverse waves *vs.* (m s^{-1}), sound velocities of longitudinal waves v_l (m s^{-1}), average velocities v_m (m s^{-1}) and Debye temperatures $\theta(D)$ (K) of the compounds

Comp.	ρ	v_l	v_s	v_m	$\theta(D)$
$LaIn_3$	7.316 (7.45[a])	3551.97	1871.88	2092.91	130.18
$CeIn_3$	7.661	3600.34	1904.86	2166.58	136.73
$PrIn_3$	7.737	3421.79	1916.10	2132.72	134.78
$NdIn_3$	7.871	3439.08	1900.38	2117.45	134.46
$LaSn_3$	7.358 (7.46[a])	3269.06	1689.14	1891.06	116.92
$CeSn_3$	7.664	3902.84	2165.59	2412.16	151.05
$PrSn_3$	7.804	3323.42	1794.79	2003.25	126.14
$NdSn_3$	7.936	3375.35	1908.81	2122.88	134.12

[a] Ref. 3.

IV. Conclusions

In summary, we have performed theoretical analyses of the structural, electronic and elastic properties of RIn_3 and RSn_3 (R = La, Ce, Pr and Nd) using density functional theory. The calculated structural properties of the compounds are consistent with experimental results. The density of states and band structures reveal the intermetallic nature of these compounds. It is concluded that the spin–orbit coupling effect, which is a correction to the Schrödinger wave equation, enhances as one goes from La to Nd in a compound, which demonstrates the interesting nature of this effect in the periodic table. We discussed the influence of the spin–orbit coupling strength on the band structure. Mechanical properties were also evaluated using elastic constants. From the calculated elastic properties and other mechanical properties, all of the compounds investigated are found to be ductile in nature with elastic anisotropy.

References

1 S. Ram, V. Kanchana, G. Vaitheeswaran, A. Svane, S. B. Dugdale and N. E. Christensen, *Phys. Rev. B: Condens. Matter Mater. Phys.*, 2012, **85**, 174531.
2 S. Ram, V. Kanchana, A. Svane, S. B. Dugdale and N. E. Christensen, *J. Phys.: Condens. Matter*, 2013, **25**, 155501.
3 R. J. Gambmo, N. R. Stemple and A. M. Toxen, *J. Phys. Chem. Solids*, 1968, **29**, 295.
4 I. R. Harris and G. V. Raynor, *J. Less-Common Met.*, 1965, **9**, 7.
5 N. V. C. Shekar and P. C. Sahu, *J. Mater. Sci.*, 2006, **41**, 3207.
6 C. F. Li, Z. Q. Liu, P. J. Shang and J. K. Shang, *Scr. Mater.*, 2011, **65**, 1049.
7 M. A. Dudek and N. Chawla, *Intermetallics*, 2010, **18**, 1016.
8 I. N. Yakovkin, T. Komesu and P. A. Dowben, *Phys. Rev. B: Condens. Matter Mater. Phys.*, 2002, **66**, 035406.
9 S. J. Asadabadi, S. Cottenier, H. Akbarzadeh, R. Saki and M. Rots, *Phys. Rev. B: Condens. Matter Mater. Phys.*, 2002, **66**, 195103.
10 K. A. Gschneider Jr, *Solid State Phys.*, 1964, **16**, 275.

11 S. Jalali Asadabadi and H. Akbarzadeh, *Phys. B*, 2004, **349**, 76.
12 Z. Kletowski, *Solid State Commun.*, 1989, **72**, 901.
13 K. H. J. Buschow, H. W. de Wijn and A. M. van Diephen, *J. Chem. Phys.*, 1969, **50**, 137.
14 I. Umehara, N. Nagai and Y. Ōnuki, *J. Phys. Soc. Jpn.*, 1991, **60**, 1294.
15 I. Umehara, Y. Kurosawa, N. Nagai, M. Kikuchi, K. Satoh and Y. Ōnuki, *J. Phys. Soc. Jpn.*, 1990, **59**, 2848.
16 Y. Ōnuki and R. Settai, *Low Temp. Phys.*, 2012, **38**, 119.
17 N. D. Mathur, F. M. Grosche, S. R. Julian, I. R. Walker, D. M. Freye, R. K. W. Haselwimmer and G. G. Lonzarich, *Nature*, 1998, **394**, 39.
18 Z. Kletowski, *Solid State Commun.*, 1987, **62**, 745.
19 K. Kawashima, M. Maruyama, M. Fukuma and J. Akimitsu, *Phys. Rev. B: Condens. Matter Mater. Phys.*, 2010, **82**, 094517.
20 A. Freeman and D. Koelling, *J. Phys.*, 1972, **33**, C3–C57.
21 S. D. Johnson, J. R. Young, R. J. Zieve and J. C. Cooley, *Solid State Commun.*, 2012, **152**, 513.
22 W. R. Johanson, G. W. Crabtree, A. S. Edelstein and O. D. MacMasters, *Phys. Rev. Lett.*, 1981, **45**, 504.
23 R. Settai, K. Sugiyama, A. Yamaguchi, S. Araki, K. Miyake, T. Takeuchi, K. Kindo, Y. Ōnuki and Z. Kletowski, *J. Phys. Soc. Jpn.*, 2000, **69**, 3983.
24 K. A. Gschneider Jr, S. K. Dhar, R. J. Stierman, T. W. E. Tsang and O. D. MacMasters, *J. Magn. Magn. Mater.*, 1985, **47 & 48**, 51.
25 A. P. Murani, *Phys. Rev. B: Condens. Matter Mater. Phys.*, 1983, **28**, 2308.
26 Y. Ōnuki and R. Settai, *Low Temp. Phys.*, 2012, **38**, 89.
27 T. Iizuka, T. Mizuno, B. Hun Min, Y. S. Kwon and S. ichi Kimura, *J. Phys. Soc. Jpn.*, 2012, **81**, 043703.
28 J. A. Abraham, G. Pagare, S. S. Chouhan and S. P. Sanyal, *Comput. Mater. Sci.*, 2014, **81**, 423.
29 J. A. Abraham, G. Pagare, S. S. Chouhan and S. P. Sanyal, *Intermetallics*, 2014, **51**, 1.
30 P. Blaha, K. Schwarz, G. k. H. Madsen, D. Kuasnicka and J. Luitz, *WIEN2K, an augmented plane wave + local orbitals program for calculating crystal properties*, K. Schwarz, Technical Universitat, Wien, Austria, 2001.
31 O. K. Andersen, *Phys. Rev. B: Solid State*, 1975, **12**, 3060.
32 J. P. Perdew and A. Zuanger, *Phys. Rev. B: Condens. Matter Mater. Phys.*, 1981, **23**, 5048.
33 J. P. Perdew, K. Burke and M. Ernzerhop, *Phys. Rev. Lett.*, 1996, **77**, 3865.
34 J. P. Perdrew, A. Ruzsinszky, G. I. Csonka, O. A. Vydrov, G. E. Scuseria, L. A. Constantin, X. Zhou and K. Burke, *Phys. Rev. Lett.*, 2008, **100**, 136406.
35 Z. Wu and R. E. Cohen, *Phys. Rev. B: Condens. Matter Mater. Phys.*, 2006, **73**, 235116.
36 A. D. Becke, *J. Chem. Phys.*, 1993, **98**, 5648.
37 J. P. Perdew, S. Kurth, A. Zupan and P. Blaha, *Phys. Rev. Lett.*, 1999, **82**, 2544.
38 Z. Ali, B. Khan, I. Ahmad, I. Khan and S. Jalali Asadabadi, *J. Magn. Magn. Mater.*, 2015, **381**, 34.
39 S. Jalali Asadabadi, *Phys. Rev. B: Condens. Matter Mater. Phys.*, 2007, **75**, 205130.
40 S. Jalali Asadabadi and F. Kheradmand, *J. Appl. Phys.*, 2010, **108**, 073531.
41 V. I. Anisimov, I. V. Solovyev, M. A. Korotin, M. T. Czyzyk and G. A. Sawatzky, *Phys. Rev. B: Condens. Matter Mater. Phys.*, 1993, **48**, 16929.
42 D. D. Koelling and B. N. Harmon, *J. Phys. C: Solid State Phys.*, 1977, **10**, 3107.
43 P. Novák, Calculation of spin-orbit coupling, 1997, http://www.wien2k.a/reg_user/textbooks/novak_lecture_on_spinorbit.ps.
44 H. J. Monkhorst and J. D. Pack, *Phys. Rev. B: Solid State*, 1976, **13**, 5188.
45 M. Jamal, S. J. Asadabadi, I. Ahmad and H. A. R. Aliabad, *Comput. Mater. Sci.*, 2014, **95**, 592.
46 R. Stadler, W. Wolf, R. Podloucky, G. Kresse, J. Furthmuller and J. Hafner, *Phys. Rev. B: Condens. Matter Mater. Phys.*, 1996, **54**, 1729.
47 M. Shafiq, S. Arif, I. Ahmad, S. Jalali Asadabadi, M. Maqbool and H. A. R. Aliabad, *J. Alloys Compd.*, 2015, **618**, 292.
48 M. Shafiq, I. Ahmad and S. J. Asadabadi, *J. Appl. Phys.*, 2014, **116**, 103905.
49 F. Birch, *Phys. Rev.*, 1947, **71**, 809.
50 K. A. Gschneidner Jr, M. Ji, C. Z. Wang, K. M. Hoa, A. M. Russell, Ya. Mudryk, A. T. Becker and J. L. Larson, *Acta Mater.*, 2009, **57**, 5876.
51 M. Zarshenas and S. J. Asadabadi, *Thin Solid Films*, 2012, **520**, 2901.
52 K. Tao, J. Zhou, Q. Sun, Q. Wang, V. S. Stepanyuk and P. Jena, *Phys. Rev. B: Condens. Matter Mater. Phys.*, 2014, **89**, 085103.
53 H. Onishi, *J. Phys.: Conf. Ser.*, 2012, **391**, 012102.
54 S. B. Dugdale, *Phys. Rev. B: Condens. Matter Mater. Phys.*, 2011, **83**, 012502.
55 C. Stassis, J. Zarestky, C. K. Loong, O. D. McMasters and R. M. Nicklow, *Phys. Rev. B: Condens. Matter Mater. Phys.*, 1981, **23**, 2227.
56 M. Born and K. Huang, *Dynamical Theory of Crystal Lattices*, Clarendon, Oxford, 1954.
57 R. Hill, *Proc. Phys. Soc., London*, 1952, **65**, 350.
58 A. Reuss, *Z. Angew. Math. Mech.*, 1929, **9**, 49.
59 W. Voigt, *Lehrburch der Kristallphysik*, Teubner, Leipzig, 1928.
60 S. F. Pugh, *Philos. Mag.*, 1954, **45**, 823.
61 V. Kanchana, *Europhys. Lett.*, 2009, **87**, 26006.
62 H. Fu, D. Li, F. Peng, T. Gao and X. Cheng, *Comput. Mater. Sci.*, 2008, **44**, 774.
63 L. Kleinman, *Phys. Rev.*, 1962, **128**, 2614.
64 V. Tvergaard and J. W. Hutchinson, *J. Am. Ceram. Soc.*, 1988, **71**, 157.
65 L. Fast, J. M. Wills, B. Johansson and O. Eriksson, *Phys. Rev. B: Condens. Matter Mater. Phys.*, 1995, **51**, 17431.
66 J. P. Sanchez, J. M. Friedt, G. K. Shenoy, A. Percheron and J. C. Achard, *J. Phys. C: Solid State Phys.*, 1976, **9**, 2207.